INORGANIC CHEMISTRY FRONTIERS

RESEARCH ARTICLE

View Article Online
View Journal | View Issue

Cite this: *Inorg. Chem. Front.*, 2024, **11**, 3063

Effect of –OH on the thermal enhancement properties of NIR-II lanthanide-doped nanoparticles in water†

Yingping Huang,[a,b,c] Jie Hu,*[a,b,c] Yongwei Guo,[a,c] Zihao Wang,[a,c] Fulin Lin[a,c] and Haomiao Zhu *[a,b,c]

Received 16th January 2024,
Accepted 16th April 2024

DOI: 10.1039/d4qi00147h

rsc.li/frontiers-inorganic

Thermo-enhanced nanothermometry has attracted considerable attention owing to its high thermal sensitivity; however, most studies are focused on upconversion nanoparticles (NPs) in the form of powder. In the field of bioapplication, it is imperative to investigate the performance of NPs dispersed in aqueous solutions to expedite their *in vivo* utilization. Particularly, the influence of –OH on the thermal properties of these NPs remains unclear. Herein, we investigated the thermal properties of α-$NaYbF_4$:2%Er,2% Ce@$NaYF_4$ NPs with different shell thicknesses emitting in the second near-infrared (NIR-II) region. Both powder and aqueous solution-dispersed NPs exhibit thermal enhancements due to a reduction in the –OH content and a blue shift of –OH vibration at elevated temperatures, respectively. The observed blue shift of –OH vibration is attributed to the conversion of 4-coordinated hydrogen-bound water into 2-coordinated hydrogen-bound water. By separately introducing LiCl and D_2O to an aqueous solution, we demonstrated how the blue shift and –OH content affect the thermal enhancement factor in aqueous solutions. These findings underscore the crucial role of –OH groups in nanothermometry for bioapplications while also providing insights for designing highly thermally sensitive nanothermometers.

1. Introduction

Compared with traditional temperature measurement methods, luminescence nanothermometry is a non-contact method and could provide two-dimensional temperature measurement with microscale or nanoscale spatial resolution. Thus, luminescence nanothermometry has been considered an effective tool for temperature measurement in the fields of nanomedicine, microelectronics, diagnosis, *etc.*[1–6] Nanothermometers based on lanthanide-doped nanoparticles (LnNPs) are considered ideal temperature sensors owing to their advantages such as high photostability, high spatial resolution and long luminescence lifetime.[7] Recently, the thermal activation of upconversion luminescence in LnNPs with remarkable thermal enhancement and ultrahigh temperature sensitivity has attracted considerable attention in the field of nanothermometry.[8–13] The underlying mechanism of the thermal enhancement effect is particularly interesting. There are several explanations for this phenomenon, including crystal thermal expansion reducing the energy migration rate,[14] heat-activated surface phonons assisting energy migration[15] and heat-induced water molecule desorption from the surface.[16] The rapid desorption of water molecules attached to the surface of LnNPs at high temperatures is considered the main mechanism. At room temperature, the energy level transition of luminescent ions (sensitizers or activators) resonates with the vibration of –OH groups in water, and this non-radiative transition can directly cause the luminescence quenching of Ln^{3+};[17–20] the removal of water from the surface of LnNPs by heating can largely recover the emission intensity of Ln^{3+}.[21]

The application of thermal enhancement nanothermometers *in vivo* requires NPs dispersed in aqueous solutions with high thermal sensitivity. However, currently, the thermal enhancement phenomenon is predominantly observed in powdered upconversion LnNPs. The presence of thermally enhanced properties and the impact of –OH vibration on the thermal enhancement of LnNPs in aqueous solutions remains unknown because heat-induced water desorption from the surface of NPs does not occur in aqueous solutions. Compared with the visible light emissions of LnNPs, the emissions of

[a]*CAS Key Laboratory of Design and Assembly of Functional Nanostructures, and Fujian Key Laboratory of Nanomaterials, Fujian Institute of Research on the Structure of Matter, Chinese Academy of Sciences, Fuzhou 350002, China. E-mail: zhm@fjirsm.ac.cn, hujie@fjirsm.ac.cn*
[b]*Fujian Provincial Key Laboratory of Polymer Materials, College of Chemistry and Materials Science, Fujian Normal University, Fuzhou 350007, China*
[c]*Xiamen Key Laboratory of Rare Earth Photoelectric Functional Materials, Xiamen Institute of Rare Earth Materials, Haixi Institutes, Chinese Academy of Sciences, Xiamen, Fujian 361021, China*

† Electronic supplementary information (ESI) available. See DOI: https://doi.org/10.1039/d4qi00147h

LnNPs in the second near-infrared (NIR-II) range enable deep tissue penetration and significantly enhance imaging contrast due to the extremely low scattering of the NIR-II light.[22–24] The investigation of thermally enhanced NIR-II emission of LnNPs is crucial for their application *in vivo*. Interestingly, the NIR-II emission of erbium (Er^{3+}) ions at 1532 nm, widely used for NIR-II fluorescence imaging, has been found to be strongly affected by the –OH groups due to the quenching of two phonons caused by –OH vibrations. Meanwhile, –OH vibrations have shown temperature-dependent characteristics in the absorption spectrum of water upon heating.[25] Therefore, in this work, Er^{3+} ions were selected as the probe to study the effect of –OH vibrations on the thermo-enhanced properties of LnNPs in aqueous solutions. Due to the weak absorption of Er^{3+} at 980 nm, Yb^{3+} ions were introduced to efficiently harvest 980 nm photons and sensitize the emission of Er^{3+} at 1532 nm. The photoluminescence quantum yield (PL QY) of Yb^{3+} and Er^{3+}-codoped NPs dispersed in aqueous solutions can reach up to 5% through core–shell structure designs such as α-$NaYbF_4$:Er,Ce,Zn@$NaYF_4$.[26] This high emission efficiency facilitates the study of thermal enhance luminescence of LnNPs in aqueous solutions.

In this work, we synthesized NIR-II α-$NaYbF_4$:2%Er,2% Ce@$NaYF_4$ NPs with different shell thicknesses and conducted a comprehensive investigation into the relationship between the PL lifetime and temperature for both powder and solution-dispersed NPs. The thermo-enhanced PL lifetime was observed under these two conditions. The change in the PL lifetime of powder NPs is related to water desorption, while in solution it is mainly influenced by –OH vibrations. Moreover, we found that altering the concentration of LiCl or decreasing the content of –OH (by adding D_2O) in the solution could induce a blue shift of the –OH vibration band and change the thermal enhancement factor of NPs. Our findings extend the understanding of the thermo-enhanced luminescence of NPs emitting in the NIR-II region, particularly in aqueous solutions, which is pivotal for their *in vivo* application.

2. Experimental

2.1. Materials

Y_2O_3 (99.999%), Yb_2O_3 (99.999%), Er_2O_3 (99.999%), Ce_2O_3 (99.999%), sodium trifluoroacetate (NaTFA), D_2O (99.99%), LiCl (99.999%), C_2H_5OH (99.7%), chloroform, cyclohexane (99.5%), and trifluoroacetic acid (TFA) were purchased from Sinopharm Chemical Reagent Co., Ltd, Shanghai, China. DSPE-PEG_{2000}-COOH (99%) was purchased from Ponsure Biotechnology Co., Ltd, Shanghai, China. Oleic acid (OA, >90%), oleylamine (OM, >70%) and 1-octadecence (ODE, >90%) were purchased from Sigma Aldrich, China. RE_2O_3 was purchased from Sinopharm Chemical Reagent Co., Ltd, Shanghai, China. All materials were used as received without further purification.

$RE(TFA)_3$ was prepared by dissolving RE_2O_3 in TFA. In a typical process, Y_2O_3 was added into a solution containing slightly excessive TFA with continuous stirring, which was kept refluxing until an optically transparent solution was formed. Then, the water bath of rotary evaporator was heated at 75 °C to remove the unreacted trifluoroacetic acid and excess water, and the resulting solution was filtered to remove the insoluble materials and dried in a vacuum drying oven at 75 °C to obtain $Y(TFA)_3$ powders. Other lanthanide trifluoroacetic salts were prepared following a similar procedure.[27]

2.2. Synthesis of α-$NaYbF_4$:2%Er,2%Ce core NPs

$Yb(TFA)_3$, $Er(TFA)_3$, $Ce(TFA)_3$, $Y(TFA)_3$ and NaTFA were prepared according to the previously reported method. α-$NaYbF_4$:2%Er,2%Ce (the contents of rare earth elements are in molar fraction) core NPs were synthesized according to the previously reported method.[28] In a typical procedure, in a 100 mL three-necked flask, a mixture of $Yb(TFA)_3$ (0.96 mmol), $Er(TFA)_3$ (0.02 mmol), $Ce(TFA)_3$ (0.02 mmol), NaTFA (1 mmol), OA (6 mL), OM (6 mL) and ODE (15 mL) was taken. The resulting solution was thoroughly stirred at room temperature for 1 h, and then the reaction solution was heated at 120 °C under vacuum for 60 min to completely remove impurities. Afterwards the reaction solution was heated to 300 °C at a rate of ~10 °C min^{-1} and reacted for 30 min in a N_2 atmosphere. After cooling down to room temperature, the products were precipitated with ethanol and obtained by centrifugation at 7500 rpm for 8 min. The obtained α-$NaYbF_4$:2%Er,2%Ce core was washed several times with ethanol and then dispersed in 10 mL cyclohexane for further use.

2.3. Synthesis of α-$NaYbF_4$:2%Er,2%Ce@$NaYF_4$ core–shell NPs

The synthesis and purification of α-$NaYbF_4$:2%Er,2% Ce@$NaYF_4$ NPs are similar to those of α-$NaYbF_4$:2%Er,2%Ce NPs, and the core–shell NPs with different inert shell thicknesses of 0.9, 1.8, 2.8, 3.6, and 8.8 nm were synthesized *via* varying the amount of reaction raw materials. Namely, a mixture of $Y(TFA)_3$ (0.5, 1.0, 2.0, 3.0, and 5.0 mmol), NaTFA (0.5, 1.0, 2.0, 3.0, and 5.0 mmol), OA (5, 10, 10, 15, and 20 mL) and ODE (5, 10, 10, 15, and 20 mL) were added in a 50/100 mL three-necked flask, respectively, and then α-$NaYbF_4$:2%Er,2% Ce core NPs (1.0 mmol) dispersed in cyclohexane were added. The resulting mixture was heated at 120 °C under vacuum for 60 minutes to completely remove impurities. The mixture was further heated at 300 °C for 1 h in a N_2 atmosphere. The products were precipitated with ethanol and obtained by centrifugation (7500 rpm) after the reaction mixture naturally cooled down to room temperature. Finally, the resulting NPs were washed several times and redispersed in 10 mL cyclohexane for further use. After centrifugation and drying, the concentration of NPs dispersed in cyclohexane was calculated to be approximately 40 mg mL^{-1}.

2.4. Synthesis of carboxyl-modified PEG ligand-coated NPs (NPs@PEG)

NPs@PEG were synthesized according to the methods reported in the literature.[29,30] Typically, the OA-capped NPs (2 mL of

10 mL was centrifuged in one pot, 40 mg mL^{-1}) in 2.0 mL of chloroform were mixed with a chloroform solution (3 mL) containing 50 mg PEG (DSPE-PEG_{2000}-COOH) in a screw-neck glass bottle (50 mL). The glass bottle was left open in a fume hood at room temperature to evaporate the chloroform slowly. The obtained mixed film was heated at 70 °C for 12 h to completely remove the chloroform. Then the film was hydrated with ultra-pure water (2 mL), and the NPs became soluble after vigorous sonication, which were further stirred at 70 °C for 10 h. The solution was transferred to a centrifuge tube and centrifuged lightly (800 rpm, 5 min). The sediment was discarded to remove possible large aggregates. Excess lipids were purified from NPs@PEG by ultracentrifugation (10 000 rpm, 5 min) and washing.

2.5. Instrumentation and Characterization

Powder X-ray diffraction (XRD) patterns of the samples were recorded using a powder X-ray diffractometer (DMAX 2400 PC, Rigaku, Japan) at a scanning rate of 8° min^{-1} in the 2θ range from 10° to 60° with Cu Kα radiation (λ = 0.154187 nm) at room temperature. The morphology of the NPs was analyzed using a transmission electron microscope (TEM, JEOL-2100F, JEOL Ltd, Japan) at 200 kV. Variable temperature steady-state and transient photoluminescence (PL) measurements were carried out using a spectrometer (FLS980, Edinburgh Instrument, UK) under 980 nm diode laser excitation. Dynamic light scattering (DLS) and zeta potential experiments were conducted using a NanoBrook Omni (BrookHaven, USA). Fourier transform infrared (FTIR) spectra in a N_2 environment were recorded using a Thermo Scientific Nicolet iS50 spectrometer (Thermo Fisher, USA). In situ Raman spectra were recorded using a Laser Microscopic Confocal Raman Spectrometer (LabRAM HR-800, Japan).

2.6. Statistical analysis

Statistical analysis was performed using Origin. The error bars in the corresponding figures were obtained based on the standard error during the fitting of the decay curve lifetime or Raman spectra.

3. Results and discussion

3.1. Synthesis and optical properties of α-$NaYbF_4$:2%Er,2%Ce@$NaYF_4$ NPs

Before commencing, it is imperative to go fast through the emission mechanism of Er^{3+}, Yb^{3+} and Ce^{3+} co-doped systems under excitation at 980 nm. Fig. 1a shows the energy levels of Er^{3+}, Yb^{3+} and Ce^{3+}. The 980 nm photons are mainly absorbed by Yb^{3+} and then transferred to the $^4I_{11/2}$ state of Er^{3+} by the Föster resonant energy transfer from the $^2F_{5/2}$ of Yb^{3+}. Subsequently, electron transitions to the $^4I_{13/2}$ state of Er^{3+} *via* nonradiative relaxation, generating 1532 nm downconversion emission from $^4I_{13/2} \rightarrow {}^4I_{15/2}$ transition. The Ce^{3+} ions are used to accelerate the nonradiative relaxation of $^4I_{11/2} \rightarrow {}^4I_{13/2}$ transition, and thus, to boost the emission of 1532 nm.[31–34] An inert shell were used to reduce the PL quenching caused by surface defects and –OH groups.[33] In addition, we compared the emission of Er^{3+} with the absorption of water in the range of 1200–1700 nm (NIR-II region) (Fig. 1b). It can be seen that the emission band of Er^{3+} overlaps with the absorption spectrum of water, indicating a significant influence of water on the emission properties of Er^{3+}, particularly in terms of spectral shape. Therefore, the thermo-enhanced PL analysis of NPs will mainly focus on investigating the PL lifetime, as it remains unaffected by the NP concentration, excitation intensity, biological tissue thickness and background interference.[35]

We first synthesized α-$NaYbF_4$:2%Er,2%Ce@$NaYF_4$ core–shell NPs by a thermal decomposition method. Further coating of the $NaYF_4$ inert layer can effectively reduce the surface defects of NPs, thus increasing the PL intensity. A series of α-$NaYbF_4$:2%Er,2%Ce@$NaYF_4$ NPs with different inert shell thicknesses can be obtained by simply changing the amount of $NaYF_4$. The transmission electron microscopic (TEM) images and size distribution statistics of these NPs are shown in Fig. 1c and S1a, b,† illustrating their exceptional uniformity and monodispersity. The thickness of the inert shell in the synthesized core–shell NPs was estimated to be 0.9, 2.8, 3.6, 4.9 and 8.8 nm, respectively. These NPs were named CS1, CS2, CS3, CS4 and CS5 accordingly. The XRD patterns of the core and core–shell NPs confirm the formation of the pure α-$NaYF_4$ structure because of the negligible lattice mismatch between α-$NaYbF_4$ and α-$NaYF_4$ (Fig. 1d).[32,34] The corresponding high-resolution transmission electron microscopic (HRTEM) image shows the high crystallinity of NPs (Fig. 1c). The lattice spacing of the shell is ~3.13 Å (Fig. 1c), which matches well with the (101) plane of α-$NaYF_4$ (PDF#16-0034). The high-angle annular dark field-scanning TEM (HAADF-STEM) of NPs clearly shows the core–shell structure of the NPs (Fig. 1c). In order to obtain a good dispersibility of NPs in water, these NPs were surface functionalized with DSPE-PEG_{2000}-COOH. The Fourier transform infrared (FTIR) spectra of NPs before and after coating are shown in Fig. S2a,† it can be seen that a new –OH vibration around 3450 cm^{-1} and –C═O vibration at 1733 cm^{-1} appeared after functionalization.[36] This confirmed the successful coating of DSPE-PEG_{2000}-COOH on NPs. Dynamic light scattering (DLS) measurements show that the NPs exhibit a mean hydrodynamic diameter in the range of 100–200 nm (Fig. S2b†), which demonstrated a good dispersibility of NPs in water.

3.2. Temperature-dependent thermal enhancement factor of NPs in the form of powder

The temperature-dependent PL lifetime of NPs with different shell thicknesses in the form of powder is shown in Fig. 2a and b; the PL intensity and PL lifetime around 1532 nm ($^4I_{13/2} \rightarrow {}^4I_{15/2}$) show a gradual increase with the increase in temperature from 20 to 100 °C. This is the same trend as observed in $LiErF_4$@$LiYF_4$ [37] and β-$NaYbF_4$,[38] which can be explained by the reduced number of –OH attached to the NPs with the increase in temperature. We measured the FTIR spectrum of

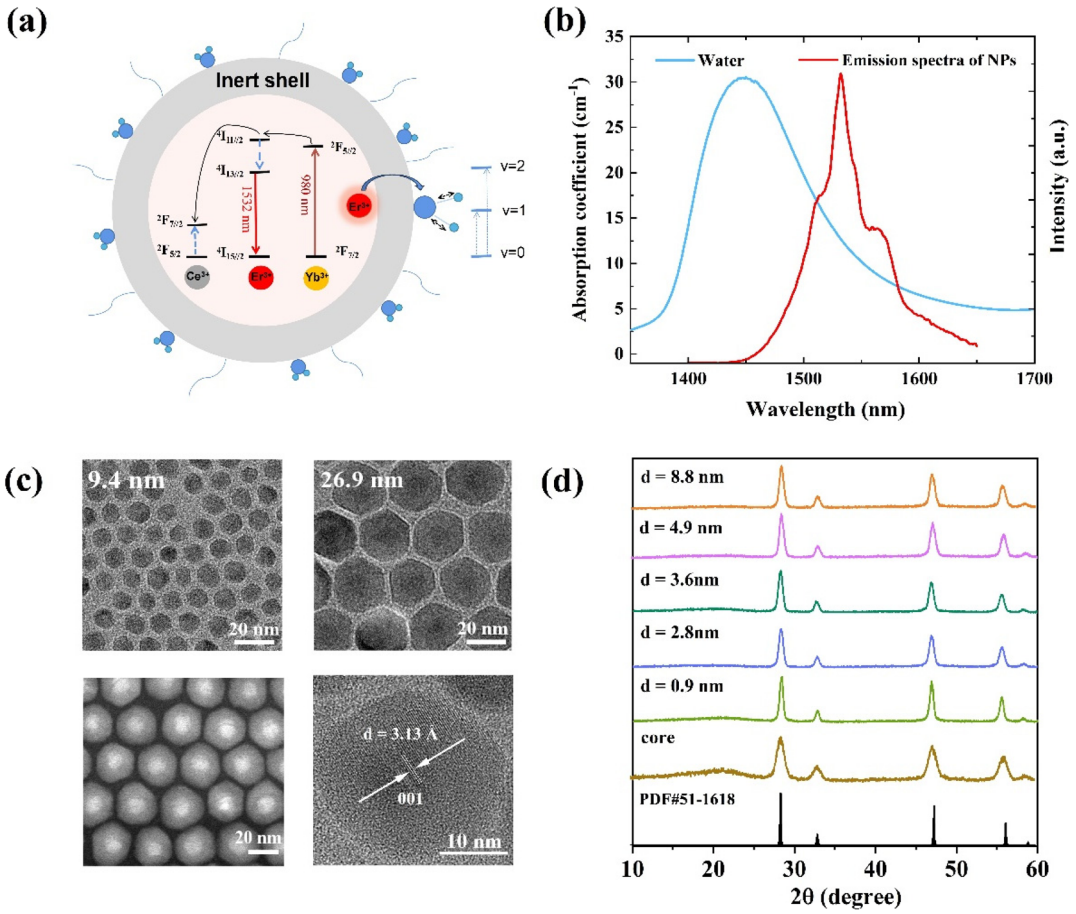

Fig. 1 (a) Energy level diagram illustrating the PL process of core–shell NPs. (b) Absorption spectra of water and emission spectra of α-$NaYbF_4$:2% Er,2%Ce@$NaYF_4$ NPs under excitation at 980 nm in the range of 1300–1700 nm. (c) TEM images of the as-prepared α-$NaYbF_4$:2%Er,2%Ce core NPs (9.4 nm) and α-$NaYbF_4$:2%Er,2%Ce@$NaYF_4$ core–shell NPs (26.9 nm); the corresponding HAADF-STEM and high-resolution TEM images of the α-$NaYbF_4$:2%Er,2%Ce@$NaYF_4$ (26.9 nm) NPs. (d) XRD patterns of the α-$NaYbF_4$:2%Er,2%Ce core and α-$NaYbF_4$:2%Er,2%Ce@$NaYF_4$ core–shell NPs with different shell thicknesses (*d* = 0.9, 2.8, 3.6, 4.9, and 8.8 nm). The card PDF#51-1618 is from α-$NaYbF_4$.

NPs as a function of temperature, as shown in Fig. 2c. Notably, the stretch intensity of –OH around 3400 cm^{-1} shows a huge decrement with the increase in temperature, while –CH and –COOH groups remain relatively stable. This observation confirms that –OH has a strong effect on the thermal enhancement of NPs. To investigate the importance of energy migration between Ln^{3+} and –OH groups, a core–shell structure was designed to change the distance between Ln^{3+} and –OH group. As shown in Fig. S3,† the PL lifetime monitored at 1532 nm increases from 2.6 to 12.1 ms when the thickness of the $NaYF_4$ shell increased from 0.9 to 8.8 nm. The long lifetime of the prepared NPs is mainly due to the f–f forbidden transition of $^4I_{13/2} \rightarrow {}^4I_{15/2}$. This transition is significantly influenced by the surface defects and ligands present on the NPs. By applying an inert shell $NaYF_4$ coating, we can effectively reduce the surface defects and increase the distance between luminescence centers and surface quenchers. Consequently, this leads to a reduction in surface quenching. As we can see, the increased thickness of the inert shell leads to prolonged lifetimes of NPs. Then we studied the temperature-dependent lifetime of these NPs, as shown in Fig. S3.† In this case, the thermal enhancement factor, obtained by dividing the PL lifetime at a specific temperature by its value at 20 °C, was used to describe the variation in PL lifetime with the temperature. All the samples show the thermo-enhanced PL lifetime (Fig. S3†), but the thermal enhancement factor is quite different among different NPs (Fig. 2d). The NPs with the lowest shell thickness show the highest enhancement factor, reaching a value of 1.33 at 100 °C. The short distance between Er^{3+} ions and the –OH group in NPs with a low shell thickness explains this phenomenon, resulting in a larger quenching effect than that of other NPs at room temperature. However, the quenching effect can be mitigated by reducing the number of –OH groups upon heating, thus leading to a high thermal enhancement factor in small NPs.

3.3. Temperature-dependent thermal enhancement factor of NPs in aqueous solutions

In order to remove the influence of water desorption on the surface of NPs as a function of temperature, we investigated

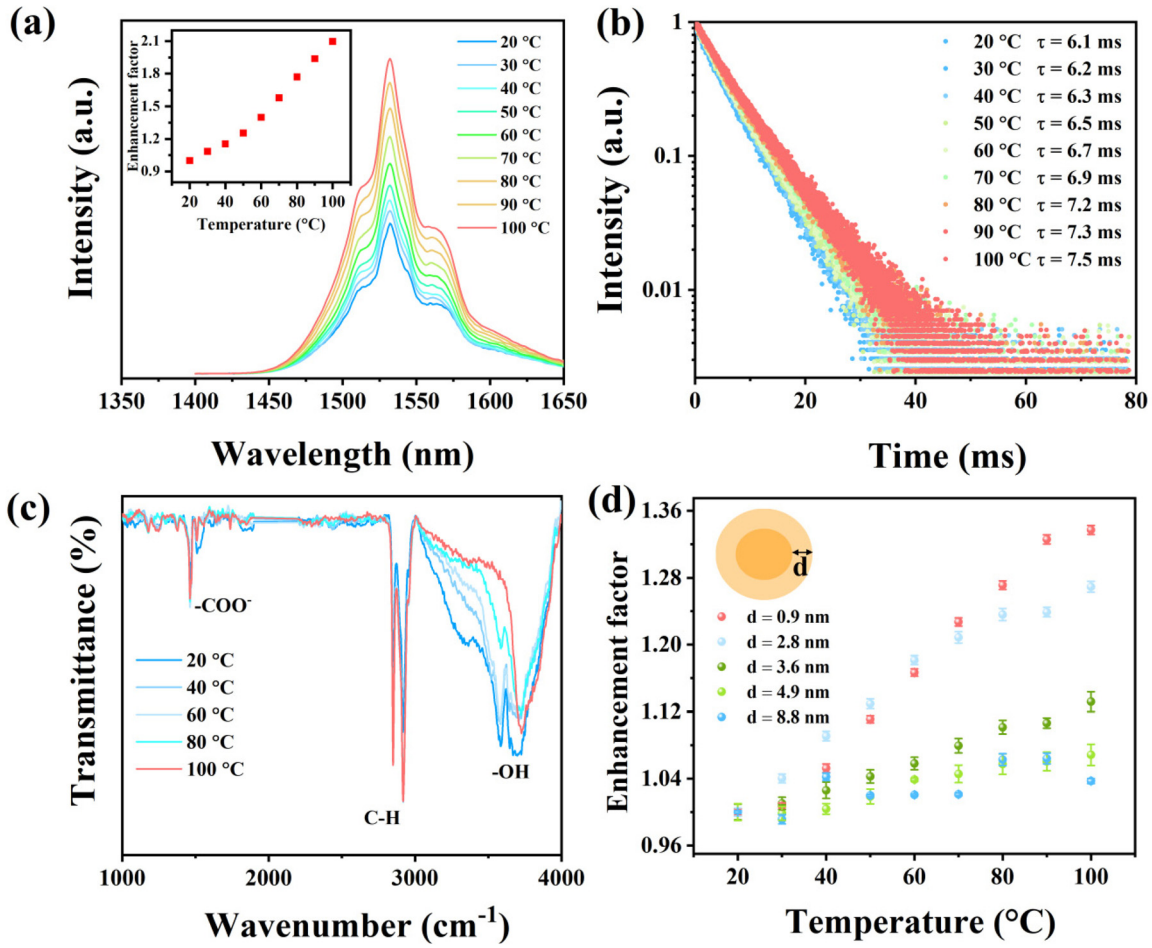

Fig. 2 (a) PL intensity and (b) PL lifetime of the α-$NaYbF_4$:2%Er,2%Ce@$NaYF_4$ core–shell NPs (16.6 nm) monitored at 1532 nm under excitation at 980 nm. (c) FTIR spectra of the α-$NaYbF_4$:2%Er,2%Ce@$NaYF_4$ core–shell NPs measured at different temperatures (20 to 100 °C). (d) Temperature-dependent thermal enhancement factor of NPs in the form of powder with different shell thicknesses (*d* = 0.9, 2.8, 3.6, 4.9, and 8.8 nm).

the temperature-dependent PL lifetime of NPs with different shell thicknesses in aqueous solutions. To assess any thermal effect caused by the 980 nm laser during the PL lifetime measurement, we examined the lifetime of NPs@PEG (*d* = 3.6 nm) in aqueous solutions at a different excitation power of 980 nm, as shown in Fig. S4.† We can see that the PL lifetime remains unchanged, suggesting that the 980 nm laser power has minimal effects on the lifetime. The temperature-dependent lifetime of NPs in aqueous solutions is shown in Fig. S5,† and their thermal enhancement factors are summarized in Fig. 3a. The thermal enhancement factor of NPs with a low shell thickness is observed to be higher, similar to our observations in the NPs in the form of powder. This phenomenon cannot be attributed to the desorption of water from the surface of NPs as these NPs are dispersed in water. In the previous report by Tamara,[25] they demonstrated that the temperature-dependent absorption of water around 1450 nm shows a blue shift with the temperature increasing from 25 to 65 °C, but the total absorption intensity remains unchanged. Therefore, we infer that the shift of –OH vibrations may play an important role in the thermal enhancement of NPs in aqueous solutions.

To reveal the variation in –OH stretch vibration with temperature, we measured the temperature-dependent Raman spectra of water, as shown in Fig. 3b, where we observed an –OH stretch vibration frequency ranging from 3000 to 3700 cm^{-1}. Additionally, with the increase in temperature, the shape of the –OH stretch becomes narrower and displays a blue shift. The Gaussian fitting shows that the stretching of the –OH band can be divided into three bands at 3226 cm^{-1}, 3439 cm^{-1} and 3610 cm^{-1} (Fig. S6†), corresponding to 4-coordinated hydrogen-bonded water (4-HB·H_2O), 2-coordinated hydrogen-bonded water (2-HB·H_2O) and nonhydrogen-bonded water, respectively.[39–41] With the increase in temperature, the component of 3226 cm^{-1} band decreased, while the component of 3439 cm^{-1} increased. Meanwhile, the component of 3610 cm^{-1} remains almost stable (Fig. 3c and Table S1†). These observations suggest the transition of 4-coordinated hydrogen-bonded water to 2-coordinated hydrogen-bonded water as the temperature increases.[40] The energy gap between $^4I_{13/2}$ and $^4I_{15/2}$ states of Er^{3+} was estimated to be 6527 cm^{-1} (emission peak at 1532 nm), which matches the two-phonon vibration of –OH in 4-coordinated hydrogen-bonded water

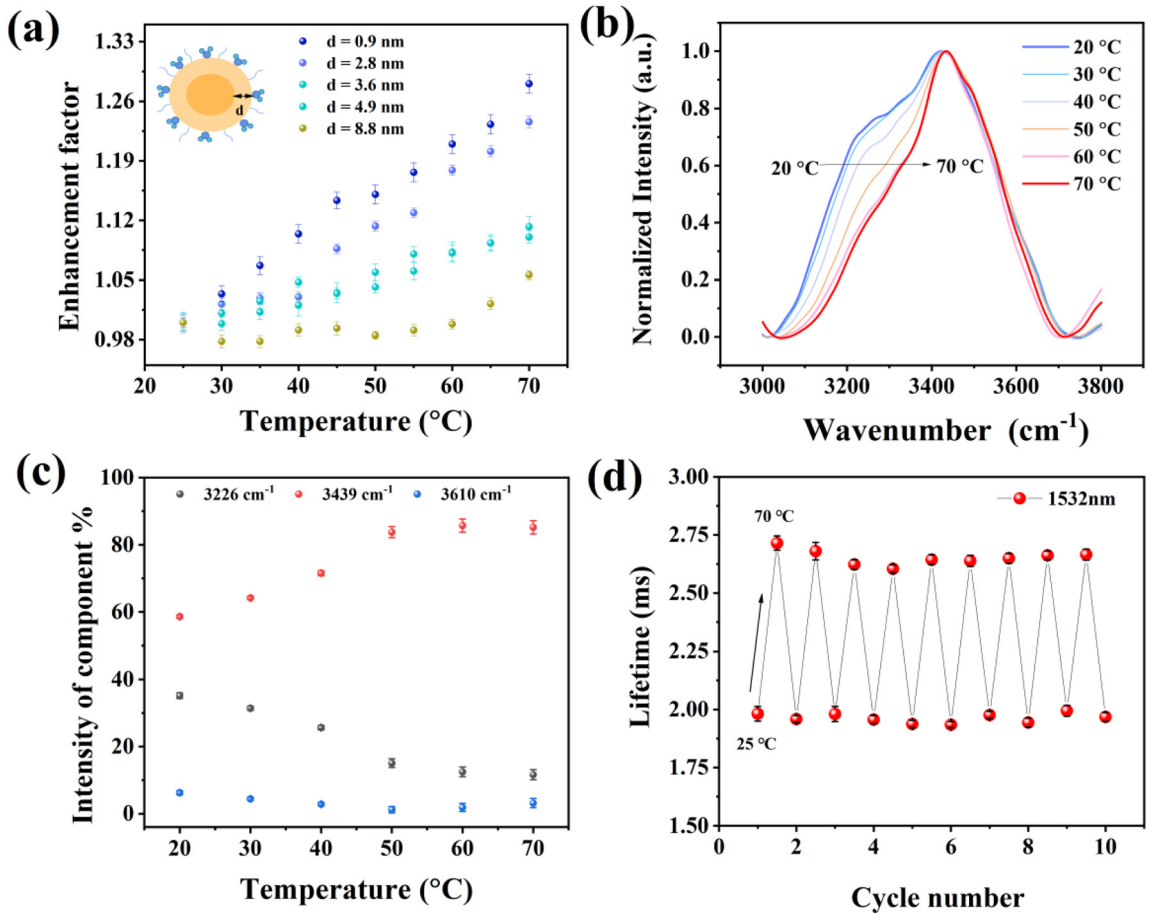

Fig. 3 (a) Temperature-dependent thermal enhancement factor of NPs@PEG dispersed in an aqueous solution with different shell layer thicknesses (d = 0.9, 2.8, 3.6, 4.9, and 8.8 nm) monitored at 1532 nm under excitation at 980 nm. (b) Raman spectra of NPs@PEG (d = 3.6 nm) measured at different temperatures (20 to 70 °C). (c) Effects of temperature on three deconvoluted Gaussian components (3226 cm^{-1}, 3439 cm^{-1}, and 3610 cm^{-1}) of Raman spectra of NPs@PEG (d = 3.6 nm) dispersed in an aqueous solution. (d) Repeatability of the PL lifetime of NPs@PEG (d = 3.6 nm) in 9 heating-cooling cycles.

(3226 cm^{-1}). With the increase in temperature, the transition of 4-coordinated hydrogen-bonded water (3226 cm^{-1}) to 2-coordinated hydrogen-bonded water (3439 cm^{-1}) increases the energy mismatch between $^4I_{13/2} \rightarrow {}^4I_{15/2}$ transition of Er^{3+} and two-phonon vibration of –OH, leading to reduced energy transfer from $^4I_{13/2}$ to the two-phonon vibration of –OH, thereby, prolonging the PL lifetime of Er^{3+} emitted at 1532 nm. The stability and repeatability are crucial parameters for the application of nanothermometers. To assess this, we measured the PL lifetime of NPs during 9 heating and cooling cycles between 25 and 70 °C (Fig. 3d). Remarkably, no significant change was observed, thus demonstrating the good stability of our NPs.

3.4. Temperature-dependent thermal enhancement factor of NPs in LiCl solutions

It is clear now how the –OH stretching affects the PL lifetime of NPs in aqueous solutions at different temperatures. However, ion–water interactions are ubiquitous within the complicate biological environment. For example, Li^+, Na^+, K^+, F^-, Cl^-, Br^-, and I^- ions were found to exert an influence on water's structural arrangement,[42] and they were classified as kosmotropes (structure makers) or chaotropes (structure breakers) according to their interaction with water. Therefore, it is necessary to comprehend the impact of ions on the thermal enhancement factor of NPs in solutions. In this case, we used a LiCl solution instead of the NaCl solution as the NPs have superior dispersibility in the LiCl solution over the NaCl solution. NPs@PEG (d = 3.6 nm) was selected to study the impact of ions on the –OH vibration and, thus, the PL lifetime of NPs, owing to their relatively good thermal enhancement factor and luminescence intensity. As shown in Fig. 4a, the PL lifetime of NPs gradually increased with the increase in LiCl mass concentration. This phenomenon can be explained by the decreased –OH stretching at low wavenumber (Fig. 4b). To go in deeper, the Raman spectra of –OH in the LiCl solution were fitted by three bands: 3226 cm^{-1}, 3439 cm^{-1} and 3610 cm^{-1} (Fig. S7 and Table S2†). Notably, the intensity of the –OH vibration band around 3226 cm^{-1} decreased with the increment in LiCl concentration. This observation supports that both LiCl and

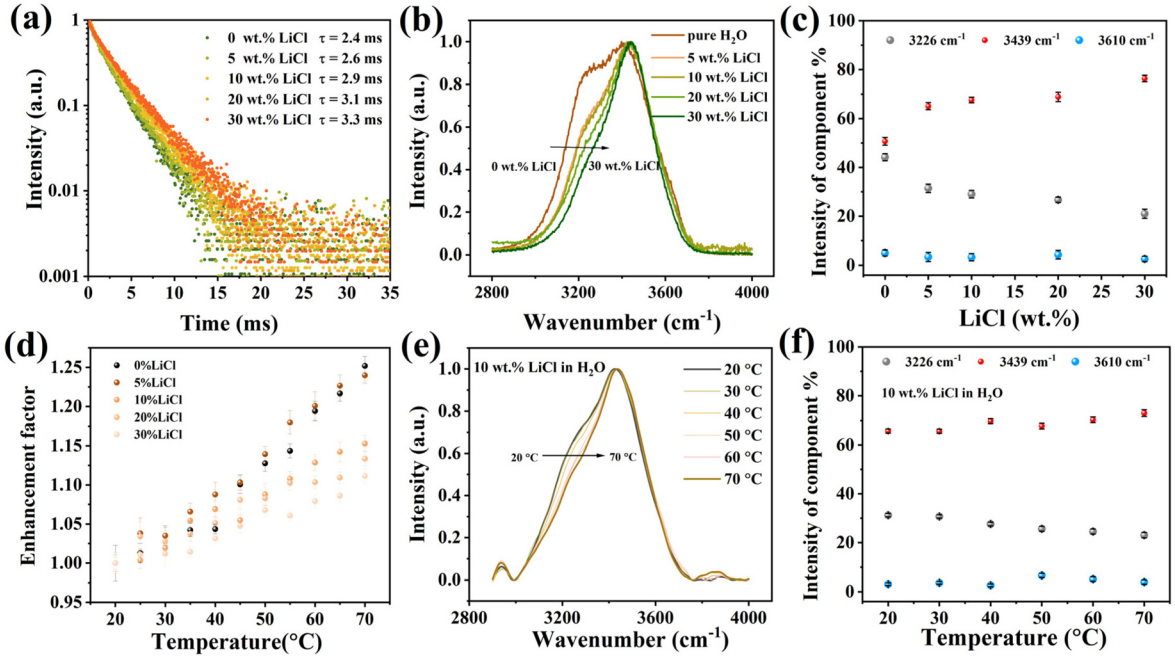

Fig. 4 (a) PL decay curves of NPs@PEG (d = 3.6 nm), which were dispersed in different concentrations of LiCl solutions monitored at 1532 nm under excitation at 980 nm. (b) Raman spectra of NPs@PEG (d = 3.6 nm) dispersed in different concentrations of LiCl solution. (c) Effects of LiCl mass concentration on three deconvoluted Gaussian components (3226 cm^{-1}, 3439 cm^{-1}, and 3610 cm^{-1}) of the Raman spectra of LiCl solution. (d) Temperature-dependent thermal enhancement factor of NPs@PEG (d = 3.6 nm), which were dispersed in different concentrations of LiCl solution monitored at 1532 nm under excitation at 980 nm. (e) Raman spectra of NPs@PEG (d = 3.6 nm) dispersed in a 10 wt% LiCl solution measured at different temperatures (20 to 70 °C). (f) Effects of temperature on three deconvoluted Gaussian components (3226 cm^{-1}, 3439 cm^{-1}, and 3610 cm^{-1}) of Raman spectra of NPs@PEG (d = 3.6 nm) dispersed in a 10 wt% LiCl solution.

temperature have the same effect on the water structure, as shown in Fig. 4c and 3c. In other words, LiCl could also lead to the transition of 4-coordinated hydrogen-bonded water (3226 cm^{-1}) to 2-coordinated hydrogen-bonded water (3439 cm^{-1}), thus prolonging the PL lifetime of Er^{3+} at 1532 nm with the increment in LiCl concentration. We then studied how LiCl affects the thermal properties of NPs, as shown in Fig. 4d and S8.† Interestingly, the thermal enhancement factor was found to decrease with the increment in LiCl concentration. We further measured the temperature-dependent Raman spectra of NPs in a 10 wt% LiCl aqueous solution and found that the change in –OH stretch band (Fig. 4e) is smaller than that of pure water. The fitted –OH band as a function of temperature is shown in Fig. 4f, and the fitting parameters are listed in Table S3.† We can see that the component of 3226 cm^{-1} band in the LiCl solution is 31% at 20 °C, which is smaller than that in the aqueous solution (38% at 20 °C), indicating that part of water molecules have transferred to 2-coordinated hydrogen-bonded water (3439 cm^{-1}) before heating. In order to study the effect of shell thickness, we also examined the temperature-dependent PL lifetime of NPs@PEG (d = 8.8 nm) dispersed in different concentrations of LiCl solutions. As shown in Fig. S9,† the thermal enhancement factors are nearly the same for different concentrations of LiCl solutions, suggesting that the shell thickness of 8.8 nm is sufficient to suppress the impact of water.

3.5. Temperature-dependent thermal enhancement factor of NPs in a D_2O solution

To study how the number of –OH groups affects the thermal enhancement factor of the NP-dispersed solution, we prepared a series of NPs@PEG (d = 3.6 nm) solutions with different ratios of V_{D_2O}/V_{H_2O}. The PL lifetime of NPs in pure D_2O is 7.8 ms, which slightly declined with the increase in H_2O content (Fig. 5a), due to the introduction of –OH quenching ligands to the surface of NPs. It can also be explained from the Raman spectra of these solutions, as shown in Fig. 5b, and the vibration peak strength of –OD group in the range of 2000–2800 cm^{-1}, decreased obviously with the increase in water content, while the vibration intensity of –OH groups in the range of 3100–3700 cm^{-1} increases with the increase in water content. The thermo-enhanced properties of these NPs were subsequently investigated. When NPs were dispersed in a pure D_2O solution, they exhibited the original weak thermal quenching behaviour. However, with a slight increase in water content, the thermal enhancement factor increased significantly (Fig. 5c and S10†). The *in situ* Raman spectrum of an aqueous solution with a V_{D_2O}/V_{H_2O} ratio of 96/4 shows a weak blue shift of the –OH vibration band (Fig. 5d), potentially due to the destruction of the hydrogen bond with the increase in temperature. As a result, the more the –OH groups in the aqueous solution are, the better the thermal enhancement will

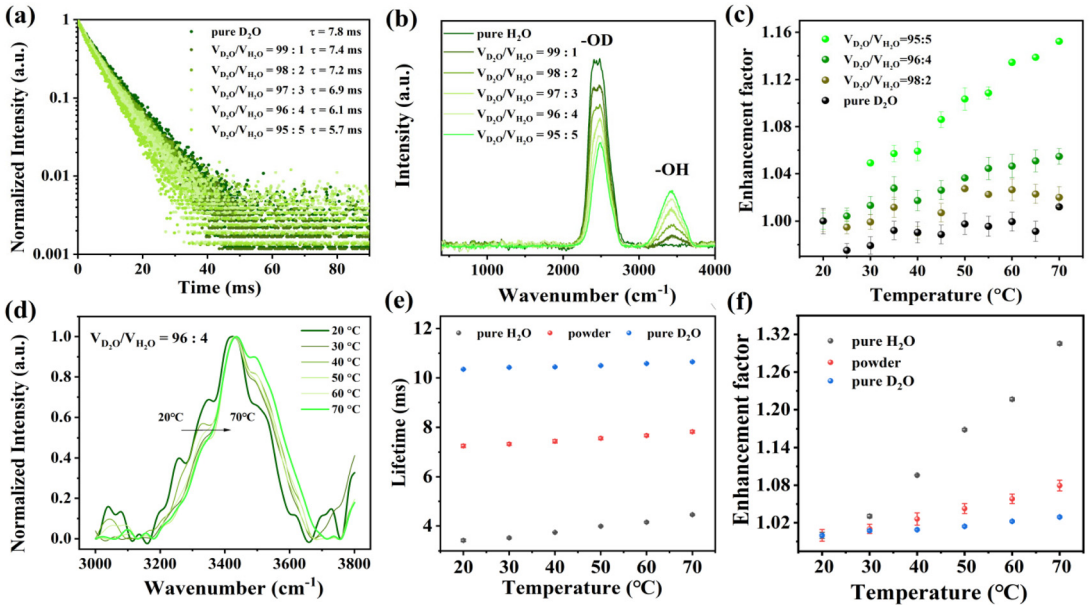

Fig. 5 (a) PL decay curves of NPs@PEG (d = 3.6 nm) in a D_2O solution, which were dispersed in different contents of H_2O monitored at 1532 nm. (b) Raman spectra of NPs@PEG (d = 3.6 nm) dispersed in different V_{D_2O}/V_{H_2O} ratio solutions. (c) Temperature-dependent thermal enhancement factors of NPs@PEG (d = 3.6 nm) dispersed in different V_{D_2O}/V_{H_2O} ratio solutions. (d) Raman spectra of NPs@PEG (d = 3.6 nm) dispersed in a solution with a V_{D_2O}/V_{H_2O} ratio of 96 : 4 at different temperatures (20 to 70 °C). (e) Temperature-dependent PL lifetime and (f) the thermal enhancement factors of NPs@PEG (d = 3.6 nm) in different states such as pure H_2O, in the form of powder and dispersed in pure D_2O.

be. However, when the V_{D_2O}/V_{H_2O} ratio decreases to 80/20, the thermal enhancement factor is the same as that of NPs in pure water (Fig. S11 and S12†), which indicates that not all the –OH groups in the aqueous solution play a role in the thermal enhancement of NPs. For comparison, we consider the temperature-dependent PL lifetime and thermo-enhanced factor of NPs in the form of powder, as well as when dispersed in H_2O and D_2O together, as shown in Fig. 5e and f. Obviously, the NPs dispersed in water show a high thermo-enhanced factor (1.3 at 70 °C) due to their high amount of –OH around NPs. The NPs dispersed in D_2O show a nearly zero thermal enhancement factor compared to that of NPs in the form of powder, which indicates a smaller amount of –OH groups on the surface of NPs in D_2O than that in the form of powder.

4. Conclusions

In summary, we have synthesized a series of α-$NaYbF_4$:2% Er,2%Ce@$NaYF_4$ NPs with different shell thicknesses, and the thermal enhancement factor of NPs was found to be strongly dependent on the shell thickness in both the powder form and aqueous solutions. This can be explained by the reduced number of –OH groups on the surface of NPs and the blue shift of the –OH vibration band upon heating. The fitting analysis of three bands indicates that the blue shift of –OH vibration band is due to the transition of 4-coordinated hydrogen-bonded water (3226 cm^{-1}) to 2-coordinated hydrogen-bonded water (3439 cm^{-1}), thereby enhancing the PL lifetime of Er^{3+} at 1532 nm with the increase in temperature. The same trend was observed in NPs dispersed the LiCl aqueous solution, in which the Cl^- ions destroy the hydrogen-bound water, and thus lead to the enhancement of lifetime. Besides, the thermal enhancement factor of NPs dispersed in the LiCl aqueous solution strongly depends on the LiCl concentration. Subsequently, we demonstrated how the number of –OH groups affects the thermal enhancement properties of NPs by changing the V_{D_2O}/V_{H_2O} ratio: a large number of –OH groups in the solution result in higher thermal enhancement. This was further confirmed by the result that NPs dispersed in water show a larger thermal enhancement factor than that of NPs in the form of powder or dispersed in the D_2O solution. Our study provides a comprehensive investigation into the influence of –OH groups on NP thermal enhancement and offers new insights for developing highly thermally sensitive nanothermometers.

Conflicts of interest

There are no conflicts to declare.

Acknowledgements

This research was supported by the National Natural Science Foundation of China (no. 12204480), the Natural Science Foundation of Fujian Province, China (no. 2021J01518), the Xiamen Municipal Bureau of Science and Technology (3502Z20231040).

References

1 J. Zhou, B. del Rosal, D. Jaque, S. Uchiyama and D. Jin, Advances and challenges for fluorescence nanothermometry, *Nat. Methods*, 2020, **17**, 967–980.
2 M. Quintanilla, M. Henriksen-Lacey, C. Renero-Lecuna and L. M. Liz-Marzan, Challenges for optical nanothermometry in biological environments, *Chem. Soc. Rev.*, 2022, **51**, 4223–4242.
3 A. Bednarkiewicz, L. Marciniak, L. D. Carlos and D. Jaque, Standardizing luminescence nanothermometry for biomedical applications, *Nanoscale*, 2020, **12**, 14405–14421.
4 C. D. S. Brites, R. Marin, M. Suta, A. C. N. Neto, E. Ximendes, D. Jaque and L. D. Carlos, Spotlight on Luminescence Thermometry: Basics, Challenges, and Cutting-Edge Applications, *Adv. Mater.*, 2023, **35**, 2302749.
5 D. H. Ortgies, M. Tan, E. C. Ximendes, B. del Rosal, J. Hu, L. Xu, X. Wang, E. Martín Rodríguez, C. Jacinto, N. Fernandez, G. Chen and D. Jaque, Lifetime-Encoded Infrared-Emitting Nanoparticles for in Vivo Multiplexed Imaging, *ACS Appl. Nano Mater.*, 2018, **12**, 4362–4368.
6 E. Ximendes, R. Marin, L. D. Carlos and D. Jaque, Less is more: dimensionality reduction as a general strategy for more precise luminescence thermometry, *Light: Sci. Appl.*, 2022, **11**, 237.
7 Q. Q. Ma, J. Wang, Z. H. Li, X. B. Lv, L. Liang and Q. Yuan, Recent Progress in Time-Resolved Biosensing and Bioimaging Based on Lanthanide-Doped Nanoparticles, *Small*, 2019, 1804969.
8 C. Mi, J. Zhou, F. Wang, G. Lin and D. Jin, Ultrasensitive Ratiometric Nanothermometer with Large Dynamic Range and Photostability, *Chem. Mater.*, 2019, **31**, 9480–9487.
9 Y. Q. Hu, Q. Y. Shao, X. Y. Deng, D. D. Song, S. Y. Han, Y. Dong and J. Q. Jiang, Thermally induced multicolor emissions of upconversion hybrids with large color shifts for anticounterfeiting applications, *J. Mater. Chem. C*, 2019, **7**, 11770–11775.
10 L. Lei, J. A. Xia, Y. Cheng, Y. S. Wang, G. X. Bai, H. Xia and S. Q. Xu, Enhancing negative thermal quenching effect via low-valence doping in two-dimensional confined core-shell upconversion nanocrystals, *J. Mater. Chem. C*, 2018, **6**, 11587–11592.
11 Q. Y. Shao, G. T. Zhang, L. L. Ouyang, Y. Q. Hu, Y. Dong and J. Q. Jiang, Emission color tuning of core/shell upconversion nanoparticles through modulation of laser power or temperature, *Nanoscale*, 2017, **9**, 12132–12141.
12 Y. B. Wang, L. Lei, R. G. Ye, G. H. Jia, Y. J. Hua, D. G. Deng and S. Q. Xu, Integrating Positive and Negative Thermal Quenching Effect for Ultrasensitive Ratiometric Temperature Sensing and Anti-counterfeiting, *ACS Appl. Mater. Interfaces*, 2021, **13**, 23951–23959.
13 R. Shi, E. D. Martinez, C. D. S. Brites and L. D. Carlos, Thermal enhancement of upconversion emission in nanocrystals: a comprehensive summary, *Phys. Chem. Chem. Phys.*, 2021, **23**, 20–42.
14 Y. H. Zhou, Y. Cheng, J. Xu, H. Lin and Y. S. Wang, Thermo-enhanced upconversion luminescence in inert-core/active-shell UCNPs the inert core matters, *Nanoscale*, 2021, **13**, 6569–6576.
15 Z. L. Ji, Y. Cheng, X. S. Cui, H. Lin, J. Xu and Y. S. Wang, Heating-induced abnormal increase in Yb^{3+} excited state lifetime and its potential application in lifetime luminescence nanothermometry, *Inorg. Chem. Front.*, 2019, **6**, 110–116.
16 J. J. Zhou, S. H. Wen, J. Y. Liao, C. Clarke, S. A. Tawfik, W. Ren, C. Mi, F. Wang and D. Y. Jin, Activation of the surface dark-layer to enhance upconversion in a thermal field, *Nat. Photonics*, 2018, **12**, 154–158.
17 C. Mi, J. J. Zhou, F. Wang and D. Y. Jin, Thermally enhanced NIR-NIR anti-Stokes emission in rare earth doped nanocrystals, *Nanoscale*, 2019, **11**, 12547–12552.
18 D. H. Li, W. R. Wang, X. F. Liu, C. Jiang and J. R. Qiu, Discovery of non-reversible thermally enhanced upconversion luminescence behavior in rare-earth doped nanoparticles, *J. Mater. Chem. C*, 2019, **7**, 4336–4343.
19 E. D. Martínez, A. F. García-Flores, A. N. Carneiro, C. D. S. Brites, L. D. Carlos, R. R. Urbano and C. Rettori, Controlling the thermal switching in upconverting nanoparticles through surface chemistry, *Nanoscale*, 2021, **13**, 16267–16276.
20 Y. Q. Hu, Q. Y. Shao, P. G. Zhang, Y. Dong, F. Fang and J. Q. Jiangtt, Mechanistic Investigations on the Dramatic Thermally Induced Luminescence Enhancement in Upconversion Nanocrystals, *J. Phys. Chem. C*, 2018, **122**, 26142–26152.
21 L. Yang, H. Wu, G. H. Pan, L. L. Zhang, H. J. Wu, Z. D. Hao, F. Liu and J. H. Zhang, Vacuum-Assisted Strong Luminescence Thermal Enhancement in $NaYF_4$:Ho^{3+}/Yb^{3+} Upconverting Nanocrystals: A Conclusive Evidence for the Effect of Water Desorption, *ACS Sustainable Chem. Eng.*, 2022, **10**, 16862–16870.
22 R. Arppe, I. Hyppänen, N. Perälä, R. Peltomaa, M. Kaiser, C. Würth, S. Christ, U. Resch-Genger, M. Schäferling and T. Soukka, Quenching of the upconversion luminescence of $NaYF_4$:Yb^{3+},Er^{3+} and $NaYF_4$:Yb^{3+},Tm^{3+} nanophosphors by water: the role of the sensitizer Yb^{3+} in non-radiative relaxation, *Nanoscale*, 2015, **7**, 11746–11757.
23 M. Patel, M. Meenu, J. K. Pandey, P. Kumar and R. Patel, Recent development in upconversion nanoparticles and their application in optogenetics: A review, *J. Rare Earths*, 2022, **40**, 847–861.
24 X. S. Cui, Y. Cheng, H. Lin, F. Huang, Q. P. Wu and Y. S. Wang, Size-dependent abnormal thermo-enhanced luminescence of ytterbium-doped nanoparticles, *Nanoscale*, 2017, **9**, 13794–13799.
25 T. Muñoz-Ortiz, L. Abiven, R. Marin, J. Hu, D. H. Ortgies, A. Benayas, F. Gazeau, V. Castaing, B. Viana, C. Chanéac, D. Jaque, F. E. Maturi, L. D. Carlos, E. M. Rodríguez and J. G. Solé, Temperature Dependence of Water Absorption in the Biological Windows and Its Impact on the Performance of Ag_2S Luminescent Nanothermometers, *Part. Part. Syst. Charact.*, 2022, **39**, 2200100.

26 Y. T. Zhong, Z. R. Ma, F. F. Wang, X. Wang, Y. J. Yang, Y. L. Liu, X. Zhao, J. C. Li, H. T. Du, M. X. Zhang, Q. H. Cui, S. J. Zhu, Q. C. Sun, H. Wan, Y. Tian, Q. Liu, W. Z. Wang, K. C. Garcia and H. J. Dai, In vivo molecular imaging for immunotherapy using ultra-bright near-infrared-IIb rare-earth nanoparticles, *Nat. Biotechnol.*, 2019, **37**, 1322–1331.

27 L. J. Wu, M. C. Jia, D. Li and G. Y. Chen, Shell Engineering on Thermal Sensitivity of Lifetime-Based NIR Nanothermometers for Accurate Temperature Measurement in Murine Internal Liver Organ, *Nano Lett.*, 2023, **23**, 2862–2869.

28 Y. Z. Shang, *Lanthanide Doped Nanoparticles for Low Threshold Upconverting Microlasers*, 2022.

29 L. L. Li, R. Zhang, L. Yin, K. Zheng, W. Qin, P. R. Selvin and Y. Lu, Biomimetic surface engineering of lanthanide-doped upconversion nanoparticles as versatile bioprobes, *Angew. Chem., Int. Ed.*, 2012, **51**, 6121–6125.

30 Y. Guo, J. Hu, P. Wang, H. Yang, S. Liang, D. Chen, K. Xu, Y. Huang, Q. Wang, X. Liu and H. Zhu, In Vivo NIR-II Fluorescence Lifetime Imaging of Whole-Body Vascular Using High Quantum Yield Lanthanide-Doped Nanoparticles, *Small*, 2023, **19**, e2300392.

31 Y. B. Li, S. J. Zeng and J. H. Hao, Non-Invasive Optical Guided Tumor Metastasis/Vessel Imaging by Using Lanthanide Nanoprobe with Enhanced Down-Shifting Emission beyond 1500 nm, *ACS Appl. Nano Mater.*, 2019, **13**, 248–259.

32 Y. T. Zhong, Z. R. Ma, S. J. Zhu, J. Y. Yue, M. X. Zhang, A. L. Antaris, J. Yuan, R. Cui, H. Wan, Y. Zhou, W. Z. Wang, N. F. Huang, J. Luo, Z. Y. Hu and H. J. Dai, Boosting the down-shifting luminescence of rare-earth nanocrystals for biological imaging beyond 1500 nm, *Nat. Commun.*, 2017, **8**, 737.

33 C. Mi, M. Guan, X. Zhang, L. Yang, S. Wu, Z. Yang, Z. Guo, J. Liao, J. Zhou, F. Lin, E. Ma, D. Jin and X. Yuan, High Spatial and Temporal Resolution NIR-IIb Gastrointestinal Imaging in Mice, *Nano Lett.*, 2022, **22**, 2793–2800.

34 F. Arteaga Cardona, N. Jain, R. Popescu, D. Busko, E. Madirov, B. A. Arús, D. Gerthsen, A. De Backer, S. Bals, O. T. Bruns, A. Chmyrov, S. Van Aert, B. S. Richards and D. Hudry, Preventing cation intermixing enables 50% quantum yield in sub-15 nm short-wave infrared-emitting rare-earth based core-shell nanocrystals, *Nat. Commun.*, 2023, **14**, 4462.

35 X. Y. Zhu, X. H. Wang, H. X. Zhang and F. Zhang, Luminescence Lifetime Imaging Based on Lanthanide Nanoparticles, *Angew. Chem., Int. Ed.*, 2022, **61**, e22209378.

36 L. Yan, J. S. Huang, Z. C. An, Q. Y. Zhang and B. Zhou, Activating Ultrahigh Thermoresponsive Upconversion in an Erbium Sublattice for Nanothermometry and Information Security, *Nano Lett.*, 2022, **22**, 7042–7048.

37 F. T. Rabouw, P. T. Prins, P. Villanueva-Delgado, M. Castelijns, R. G. Geitenbeek and A. Meijerink, Quenching Pathways in $NaYF_4$:Er^{3+},Yb^{3+} Upconversion Nanocrystals, *ACS Appl. Nano Mater.*, 2018, **12**, 4812–4823.

38 B. Chen, Y. Wang, Y. Guo, P. Shi and F. Wang, $NaYbF_4$@$NaYF_4$ Nanoparticles: Controlled Shell Growth and Shape-Dependent Cellular Uptake, *ACS Appl. Mater. Interfaces*, 2021, **13**, 2327–2335.

39 J. R. Clarkson, E. Baquero, V. A. Shubert, E. M. Myshakin, K. D. Jordan and T. S. Zwier, Laser-initiated shuttling of a water molecule between H-bonding sites, *Science*, 2005, **307**, 1443–1446.

40 G. E. Walrafen, Raman Spectral Studies of the Effects of Temperature on Water Structure, *J. Chem. Phys.*, 2004, **47**, 114–126.

41 Y.-H. Wang, S. Zheng, W.-M. Yang, R.-Y. Zhou, Q.-F. He, P. Radjenovic, J.-C. Dong, S. Li, J. Zheng, Z.-L. Yang, G. Attard, F. Pan, Z.-Q. Tian and J.-F. Li, In situ Raman spectroscopy reveals the structure and dissociation of interfacial water, *Nature*, 2021, **600**, 81–85.

42 B. Hribar, N. T. Southall, V. Vlachy and K. A. Dill, How ions affect the structure of water, *J. Am. Chem. Soc.*, 2002, **124**, 12302–12311.

